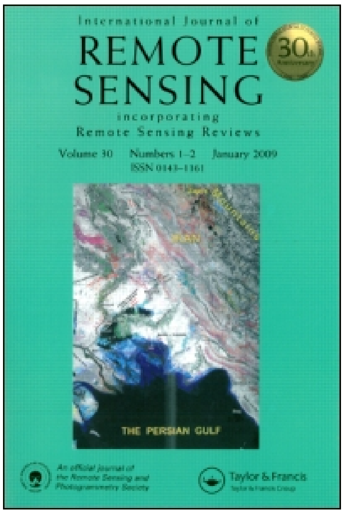

International Journal of Remote Sensing
Publication details, including instructions for authors and subscription information:
http://www.informaworld.com/smpp/title~content=t713722504

Mapping hydrologically sensitive areas on the Boreal Plain: a multitemporal analysis of ERS synthetic aperture radar data

R. B. Clark [a]; I. F. Creed [a]; G. Z. Sass [a]
[a] Department of Biology, University of Western Ontario, London, Ontario, Canada N6A 5B8

Online Publication Date: 01 January 2009

To cite this Article Clark, R. B., Creed, I. F. and Sass, G. Z.(2009)'Mapping hydrologically sensitive areas on the Boreal Plain: a multitemporal analysis of ERS synthetic aperture radar data',International Journal of Remote Sensing,30:10,2619 — 2635

To link to this Article: DOI: 10.1080/01431160802552819

URL: http://dx.doi.org/10.1080/01431160802552819

International Journal of Remote Sensing
Vol. 30, No. 10, 20 May 2009, 2619–2635

Technical Note

Mapping hydrologically sensitive areas on the Boreal Plain: a multitemporal analysis of ERS synthetic aperture radar data

R. B. CLARK, I. F. CREED* and G. Z. SASS
Department of Biology, University of Western Ontario, London, Ontario, Canada N6A 5B8

(*Received 14 July 2006; in final form 30 January 2008*)

Characterizing the spatial and temporal dynamics of hydrologically sensitive areas (HSAs) is vital to the effective management of the boreal forest. HSAs are defined as saturated or inundated areas that, if disturbed, might result in a significant change in the movement of water, nutrients and biota within landscapes. This study presents a remote sensing technique that uses archived European Remote Sensing Satellite (ERS)-1 and ERS-2 synthetic aperture radar (SAR) images to monitor HSAs in the Willow River watershed (1030 km^2) on the western Boreal Plain of Canada. ERS images were used to generate a probability of HSA occurrence map for a 10-year period (1991–2000). This map revealed the complexity of HSAs on the western Boreal Plain, where some areas remained consistently dry or wet whereas others were dynamic, transitioning from dry to wet and *vice versa*. A probability map of HSA occurrence provides spatial and temporal information previously unavailable for this region that may expand our understanding of the hydrological behaviour of drainage basins and serve as a planning tool for land management decisions.

1. Introduction

The boreal forest in Canada is facing increasing demands from various human activities such as forest harvesting and oil and gas development (Schindler 1998, Hobson *et al.* 2002). There is concern that these activities combined with substantial climatic variability and climate change will impact hydrologically sensitive areas (HSAs) within boreal landscapes (Schindler 2001, Buttle *et al.* 2005). HSAs may be defined as areas where the water table is transiently or permanently near or at the surface (saturated) or where there is ponded water (inundated). HSAs are key hydrological features regulating the horizontal movement of water, nutrients, sediment and biota within the landscape (Creed *et al.* 1996, Creed and Band 1998, Devito *et al.* 2000, Rustomji and Prosser 2001, Creed *et al.* 2003, Leibowitz and Vining 2003). For effective management of the boreal forest, maps of HSAs are needed that are spatially extensive (i.e. capture large regional drainage basins) and also reflective of the temporal dynamics of HSAs. A challenge for researchers is to develop tools that capture the spatial and temporal dynamics of HSAs at scales relevant to resource managers.

Traditionally, maps of HSAs have been restricted to provincial or federal maps that provide a snapshot in time at coarse spatial resolutions (e.g. Canada's National Topographic System (NTS)-wetlands). These maps are often derived and updated

*Corresponding author. Email: icreed@uwo.ca

International Journal of Remote Sensing
ISSN 0143-1161 print/ISSN 1366-5901 online © 2009 Taylor & Francis
http://www.tandf.co.uk/journals
DOI: 10.1080/01431160802552819

through photointerpretation of aerial photographs at scales from 1 : 65 000 to 1 : 85 000. The hydrological features (i.e. wetlands) delineated through this process are often inferred by community structure of the canopy rather than the hydrological condition on the ground surface. Photointerpretation at this scale does not capture fine-scale features and does not represent hydrological dynamics. Satellite remote sensing systems have become an important source of data for identifying and monitoring hydrological features (Pietroniro and Leconte 2005). Specifically, synthetic aperture radar (SAR) data hold promise for hydrological applications (Pietroniro and Leconte 2003). The large spatial coverage ($>100\,km^2$) and frequent satellite overpasses (24 to 35 days) of the commercially available imagery allows mapping of HSAs for regional watersheds (Oldak *et al.* 2003), including their temporal dynamics (Kasischke *et al.* 2003, Bourgeau-Chavez *et al.* 2005).

Previous studies have demonstrated the potential of SAR imagery for HSA mapping for both non-forested (Brun *et al.* 1990, Pope *et al.* 1997, Oldak *et al.* 2003) and forested (Hess *et al.* 1990, 1995, 2003, Pulliainen *et al.* 1996, Adam *et al.* 1998, Brivio *et al.* 2002, Rosenqvist *et al.* 2002, Kasischke *et al.* 2003) regions by taking advantage of two dominant scattering mechanisms that result as the surface changes from dry to saturated and then to inundated. The first scattering mechanism is primarily controlled by the dielectric properties of the surface. As the soil moisture changes from dry to saturated, its dielectric constant increases (Schmugge 1980), translating to an increase in the backscatter coefficient (Mérot *et al.* 1994, Morrissey *et al.* 1996). When soils are near saturation, the backscatter coefficient begins to level off, becoming less sensitive to any further addition of water (Kasischke *et al.* 2003). The second scattering mechanism is specular reflectance, which occurs from smooth water surfaces (Horritt *et al.* 2001). Specular reflectance occurs when the incident microwave signal is reflected away from the sensor resulting in an extremely small backscatter coefficient (Dobson and Ulaby 1986). When the ground is inundated, emergent vegetation and/or tree trunks produce double bounce scattering (Richards *et al.* 1987). Consequently, inundated soils beneath a vegetation cover generate an enhanced backscattering that can result in a significant increase in the backscatter coefficient from that of non-inundated areas (Hess *et al.* 1990, Wang *et al.* 1995, Horritt *et al.* 2003).

Several multitemporal techniques (e.g. principal component analysis) have been used to capture the spatial and temporal dynamics of HSAs. These types of approaches correlate changes in the backscatter coefficient with changes in hydrological state, thereby minimizing the need for detailed information on other parameters such as soil roughness and vegetation (Wickel *et al.* 2001). These techniques rely on the assumption of time-invariant surface properties, which is often the case for natural, undisturbed landscapes. While an absolute measure of soil moisture is not achieved, they do provide a means of monitoring spatial and temporal changes in the hydrological state (e.g. Gineste *et al.* 1998, Verhoest *et al.* 1998, Troch *et al.* 2000, Bourgeau-Chavez *et al.* 2005). Although such techniques provide both spatial and temporal information, our goal was to generate a probability map of HSA occurrence (e.g. Walter *et al.* 2000, Agnew *et al.* 2006) that offers the advantage of providing predictive information as well as representing both the spatial and temporal dynamics of HSAs. A suitable approach to achieving this is through individual image classification (e.g. Brun *et al.* 1990, Rosenqvist *et al.* 2002, Bourgeau-Chavez *et al.* 2005). Individual image classification allows for the mapping of HSAs for each SAR image date, providing a time series of HSA maps that can be used to calculate the probability of HSA occurrence. The probability map gives an easily interpretable surface, where low probability means low likelihood of observing saturated or inundated soil and high probability translates into a high likelihood of observing saturated or inundated soil. Therefore, probability maps can be readily used for the prediction of finding HSAs.

The purpose of this study was to assess the feasibility of using European Remote Sensing Satellite (ERS) SAR imagery to map the probability of HSA occurrence for a regional drainage basin on the Boreal Plain of northern Alberta, Canada. The objectives were to (1) develop a method for mapping HSAs from ERS imagery and (2) characterize the probability of HSA occurrence over a 10-year period (1991–2000). Numerous studies have suggested that the optimal SAR sensor configuration for sensing hydrological features would operate at multiple frequencies (e.g. C- and L-band) and/or multiple polarizations (e.g. HH, VV, HV) (e.g. Hess *et al.* 1995, Ulaby *et al.* 1996, Champion and Faivre 1997, Bindlish and Barros 2000). This study focused on the use of ERS SAR data because of its large archived database and the limited availability of alternative SAR data (e.g. JERS, RADARSAT and ASAR). Therefore, this study provides an assessment of whether archived ERS SAR data can be used to provide valuable hydrological information in this remote region.

2. Study area

This study was conducted in the Willow River watershed (1030 km^2), located within the mixed-wood forest in the Boreal Plain ecozone (Ecological Stratification Working Group 1996) of northern Alberta (figure 1). The watershed lies within the Peace River drainage basin and drains northeast into North Wabasca Lake near the town of Wabasca-Desmararis. The climate is continental, with long, cold winters and short, warm summers. The average annual temperature is 1°C, with monthly temperatures ranging from −16.7°C (January) to 16.5°C (July). The average annual precipitation is 475 mm, with approximately 70% of precipitation falling between May and September. The watershed is covered by thick (20 m to 230 m) glacial deposits of undifferentiated drift (Paulen *et al.* 2004*a*,*b*). The glacial history of the area has resulted in a complex spatial distribution of soils ranging from well to poorly drained Gray Luvisols and Brunisols in the uplands and Organic and Gleysols in the lowlands. The watershed has 420 m of topographic relief but most of the slopes are smaller than 5°. The forest cover is dominated by trembling aspen (*Populus tremuloides* Michx.), white spruce (*Picea glauca* (Moench) Voss) and jack pine (*Pinus banksiana* Lamb.) in the uplands, while the wettest areas are dominated by black spruce (*Picea mariana* (Mill.) B.S.P.) and tamarack (*Larix laricina* (Du Roi) K. Koch).

3. Methods

3.1 *SAR image selection and processing*

Archived ERS-1 and ERS-2 images from 1991 to 2000 were acquired from the Alaska Satellite Facility (ASF) to capture both within- and between-year variations of hydrological state (i.e. dry, mesic and wet conditions). This set of SAR images included all images from ascending and descending orbits (34 ERS-1 and 20 ERS-2) during the ice-free period (late April to early October). Image acquisition was limited to this time period because this is the most hydrologically active period of the

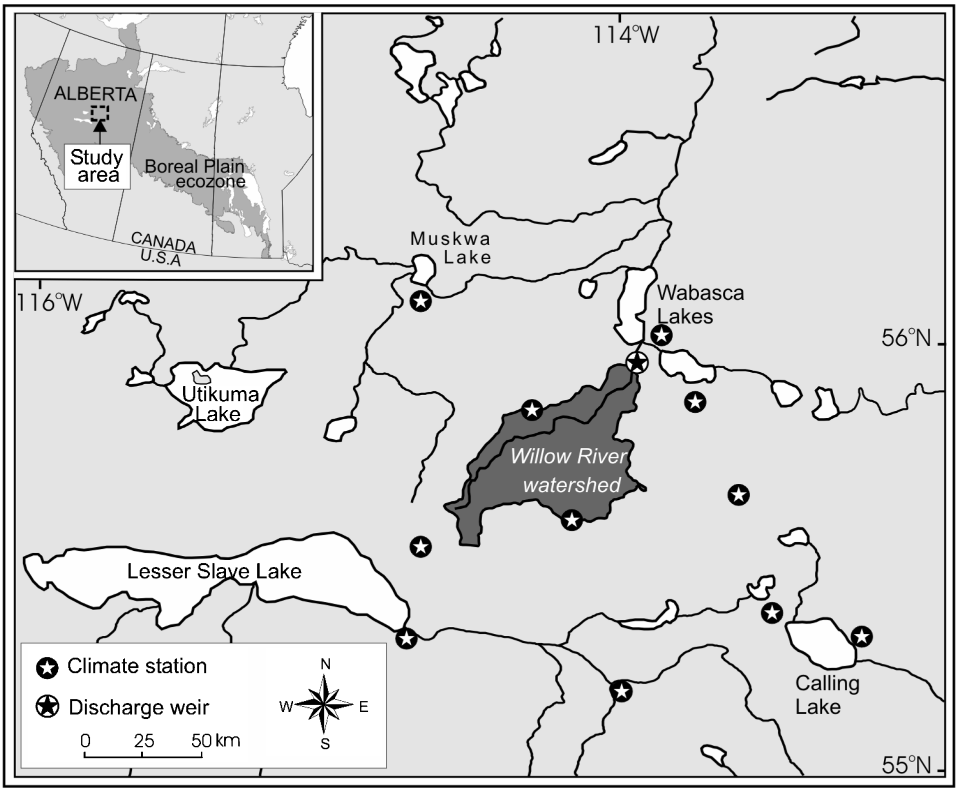

Figure 1. Map of the study area in northern Alberta, showing the Willow River watershed, meteorological stations and discharge weir. Inset: location of the Willow River watershed in the mixed-wood boreal forest on the western portion of the Boreal Plain ecozone.

year and freezing conditions outside this period substantially decrease the backscatter coefficient (Rignot and Van Zyl 1993, Morrissey *et al.* 1996), thereby precluding HSA detection.

ERS images were radiometrically calibrated using ASF software (ASF 2004). A constant +0.5 dB offset was applied to ERS-1 images to make them radiometrically comparable to ERS-2 images (Wade Albright (Data Quality Lead, ASF), personal communication). A linear correction was applied to ERS-2 images to compensate for a known loss in transmitter pulse power (Meadows *et al.* 2004). Daily correction factors were calculated from the annual rates of power loss and subsequently applied to each ERS-2 image. The outcome of the radiometric standardization was assessed by observing the stability of the average backscatter from large, uniformly distributed targets over time. We deemed the calibration process successful from the relatively steady response from distributed targets following the calibration process (figure 2). The slope of the calibrated line was not statistically different from that of a slope of zero ($p = 0.13$).

Once the ERS images were radiometrically standardized, they were orthorectified and resampled from 12.5 m to 25 m pixel spacing using a bilinear algorithm. A 3×3 gamma filter was chosen to further process the ERS images to reduce image speckle in homogeneous areas while maintaining edges and linear features (Lopes *et al.* 1993).

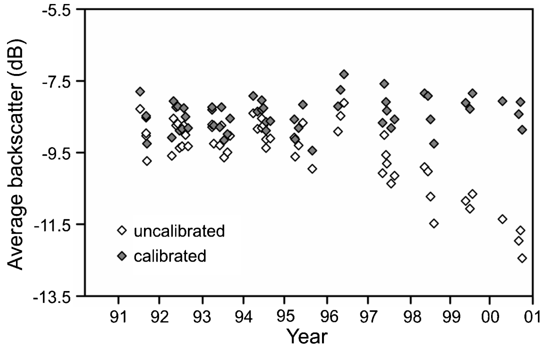

Figure 2. Average backscatter for large uniform distributed targets across the ERS scene for all image dates, before (open symbols) and after (filled symbols) radiometric calibration. The slope of the calibrated line is not statistically different from that of a slope of zero ($p=0.13$).

3.2 *Range in hydrological variability represented by the ERS imagery*

ERS image acquisition was restricted to a fixed repeat pass cycle of 35 days. The majority of images were selected between May and September with a few late April and early October images. We conducted the following analysis to confirm that the 54 images were representative of the hydrological conditions of the 10-year period from which they were selected. First, we compiled a daily time series of precipitation (P), temperature (T) and potential evapotranspiration (PET) (after Hamon 1964) for the 10-year period from 1991 to 2000 for the Willow River watershed with climate data collected from the closest meteorological stations (figure 1) (cf. Clark 2004). We also compiled a daily time series of discharge (Q) for the open water season, March to October, from a weir located near the mouth of the Willow River watershed (55° 55″ 1′ N, 113° 55″ 13′ W) (cf. Clark 2004). Second, we computed frequency distributions of P, effective precipitation (subtracting the effect of evapotranspiration) (P-PET) and Q for the day of image acquisition; the day preceding image acquisition; and cumulative 3, 7, 14 and 30 days totals preceding image acquisition. Third, we computed frequency distributions of P, P-PET and Q for all days and for cumulative 3-, 7-, 14- and 30-day totals between May 1 and September 30 from 1991 to 2000. Finally, we conducted Kolmogorov–Smirnov two-sample tests using SPSS version 13.0 (SPSS Inc., Chicago, IL, USA) to determine whether there were statistically significant differences between the frequency distributions for each hydrological variable.

3.3 *Classification of ERS imagery*

A supervised fuzzy classification approach (Zadeh 1965) was used to partition the ERS images into the two hydrological classes (i.e. inundated and saturated) used in the definition of HSAs. Each pixel of the ERS image was assigned a membership grade to each hydrological class based on a sigmoidal membership function (Burrough and McDonnell 1998) (figure 3). Membership grade ranged between 0 and 1, with 1 representing full membership (i.e. 100% probability that a pixel belonged to that particular class) and 0 representing non-membership (i.e. 0% probability that a pixel belonged to that particular class). The parameter b_x represented the crossover point on the sigmoidal curve, where the membership grade was equal to 0.5 (i.e. 50% probability that pixel belonged to that particular class)

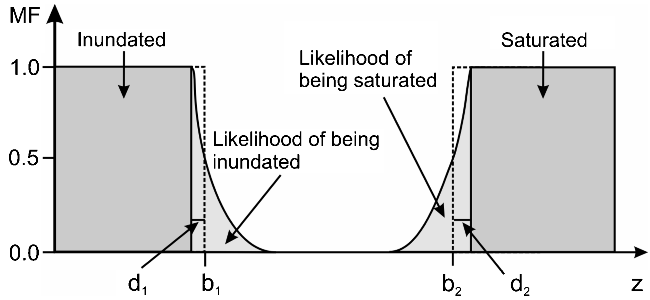

Figure 3. Fuzzy classification rules used to derive saturated and inundated areas from the ERS images.

and the parameter d_x represented the width of the transition zone (i.e. uncertainty associated in defining the class boundary) (figure 3).

The inundated class boundary (b_1=–13.8 dB) and transition zone (d_1=0.3 dB) were estimated from ERS images on days with no wind effect. An iterative approach was used where different thresholds in b_1 were set to define inundation. The spatial coincidence of inundation based on each threshold was compared to the digital lake layer from the provincial topographic map series. The threshold in b_1 that resulted in the highest spatial coincidence was used. The saturated class boundary (b_2=–7 dB) and transition zone (d_2=0.5 dB) were estimated from ERS images on days that were wet based on meteorological records. A qualitative approach was used to define b_1, where image areas with high dB (i.e. interpreted as wet) were compared to known wetland areas based on a wetland map (1 : 20 000) (L. Halsey, unpublished data) (figure 4). For both inundated and saturated classes, the transition zone parameter was set based on the nature of the class boundary. For

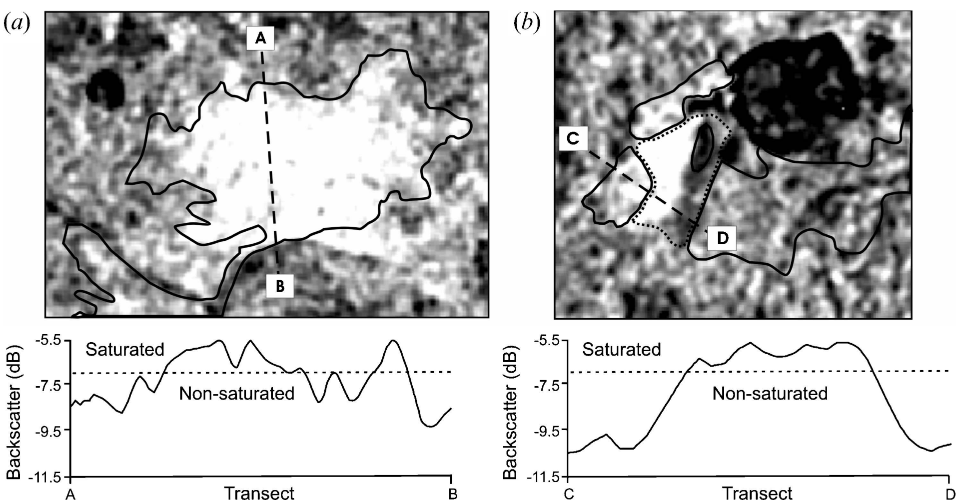

Figure 4. Fuzzy classification parameter selection for the saturated class boundary (b_2). Backscatter coefficient profile for a transect through (*a*) wooded fen and (*b*) wooded and open fen (ERS image date: 25 June 1997). The wooded fen is delineated by the solid black line, while the open fen is delineated by a fine broken line. The coarsely broken line represents the transect. The b_2 parameter threshold is indicated on the backscatter coefficient profile by the broken line, segmenting it into saturated and unsaturated. The water level for a typical fen is at or near the surface.

the inundated class, the nature of the boundary is relatively sharp, and therefore a parameter reflecting a narrow transition zone (d_1=0.3 dB) was used. By contrast, for the saturated class, the nature of the boundary is more diffuse, and therefore a parameter reflecting a wider transition zone (d_1=0.5 dB) was used.

Our selection of the backscatter coefficient for the fuzzy membership parameters are in accordance with the backscatter characteristics found in other studies. For example, a separation in the backscatter coefficient (dB) between non-saturated and saturated or non-saturated and flooded under a canopy has been reported in the range −5 to −7 dB (e.g. Brun *et al.* 1990, Adam *et al.* 1998, Townsend 2001, Horritt *et al.* 2003). The membership parameters are also in accordance with a parallel study by Sass and Creed (2008) for an adjacent watershed. Sass and Creed (2008) found that three hydrological classes (unsaturated, saturated and inundated) defined by field-based soil moisture measurements had statistically different ERS backscatter responses for similar landscape characteristics to those in this study.

Fuzzy classification was performed on all ERS images using the Terrain Analysis System (Lindsay 2005). First, membership grades were assigned to each pixel for both hydrological classes (i.e. inundated and saturated). Second, individual class layers were combined into a categorical map (inundated, saturated and non-saturated (by default)) by assigning each pixel to a class with the highest membership grade for that pixel. Third, binary maps were produced (HSA, non-HSA), where HSAs were delineated by combining the saturated and inundated classes. Mapped open-water areas with potential for wind-induced artefacts were not masked out during image classification. The large data set used in this analysis provided a sufficient number (>50%) of calm water conditions to properly identify these features.

A quantitative accuracy assessment on the individually classified maps was not undertaken. To perform such an analysis, ground-truthed data capturing the spatial and temporal patterns of HSAs from 1991 to 2000 were needed. These data were not available. However, we refer to Sass and Creed (2008), who achieved an 88% success rate in distinguishing between dry *versus* wet (saturated and inundated) areas using ERS images with similar landscape characteristics. The study by Sass and Creed (2008) was also able to capture the temporal dynamics of saturated and inundated areas over one season using ERS imagery through correlating the expansion and contraction of saturated and inundated areas to water level fluctuations of a regional lake.

3.4 *Multitemporal analysis of classified ERS images*

A map of the probability (0–100%) of HSA occurrence was generated by overlaying all 54 HSA maps, counting the number of times an HSA was present for a given pixel, and then dividing this number by the total number of images. High probabilities represented areas where the ground was frequently or permanently saturated or inundated. Low probabilities represented areas where the ground was frequently or permanently dry. If the ERS images were representative of the 10-year climate record (1991–2000), then the map reflected the probability of occurrence of an HSA for this 10-year period.

4. Results and discussion

4.1 *Capturing the range in hydrological conditions*

A single remotely sensed image represents a snapshot of the hydrological conditions at the time of imaging. A time series of remotely sensed images that is representative

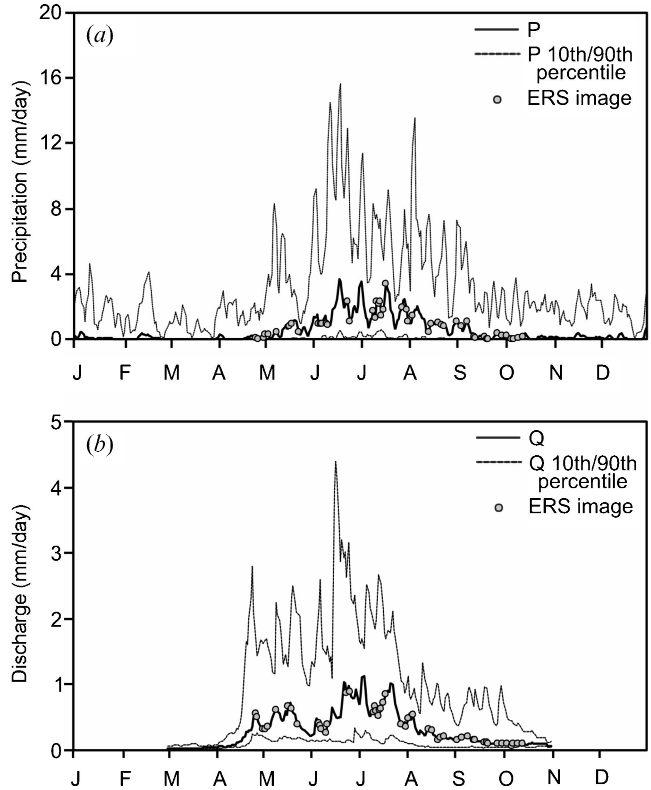

Figure 5. Timing of ERS image acquisition with respect to median daily precipitation (*a*) and discharge (*b*) with the 10th and 90th percentiles based on 10 years of meteorological data (1991–2000).

of the frequency distribution of hydrological conditions is essential for mapping the probability of HSA occurrence. We used 54 images from 1991 to 2000 that were collected from snowmelt to snowpack (figure 5) in years that were mesic (P≈PET), dry (P<PET) and wet (P>PET) (figure 6).

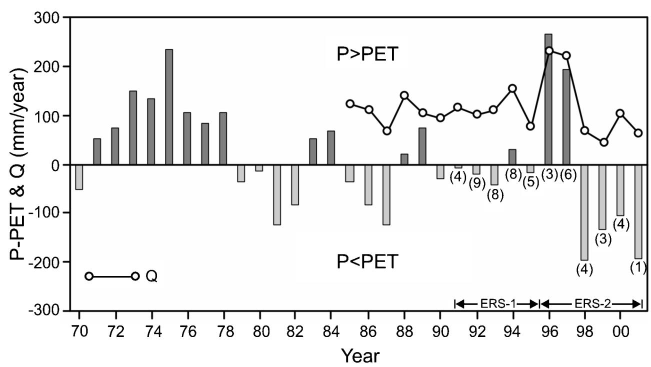

Figure 6. Annual time series (1971–2000) of precipitation minus potential evapotranspiration (P-PET) and discharge (Q) for the study area with the number of ERS images for each year in parentheses.

Table 1. Results of the Kolmogorov–Smirnov two-sample tests ($p<0.05$) showing precipitation (P), effective precipitation (P-PET) and discharge (Q) frequency distributions for the day of, and several time periods preceding, image acquisition *versus* the same frequency distributions from snowmelt to snowpack (May–September) for the 10-year period. p-values are presented, with values>0.05 indicating statistically similar distributions.

Image acquisition	P (mm/day)	P-PET (mm/day)	Q (mm/day)
Day of	0.411	0.779	0.937
1-Day preceding	0.411	0.779	0.937
3-Day preceding	0.028	0.601	0.671
7-Day preceding	0.363	0.323	0.358
14-Day preceding	0.515	0.814	0.339
30-Day preceding	0.401	0.545	0.389

Kolmogorov–Smirnov two-sample tests showed no statistically significant differences ($p<0.05$) between P, P-PET and Q frequency distributions for the day of, or the day preceding, image acquisition and the same frequency distributions for all days for snowmelt to snowpack (May–September) for the 10-year period (table 1). Similarly, there were no statistically significant differences ($p<0.05$) between P, P-PET and Q frequency distributions for the cumulative 3-, 7-, 14- or 30-day totals preceding image acquisition and the same frequency distributions for snowmelt to snowpack for the 10-year period, with one exception. The frequency distribution for the cumulative 3-day total of P preceding image acquisition was significantly different from the longer 10-year period. This may be an artefact of the data, as no other physical explanation can be provided (table 1). These results suggested that the 54 ERS images were representative of the hydrological conditions experienced over the 10-year period and offered a sufficient dataset for mapping the probability of HSA occurrence.

4.2 *Probability of formation of HSAs*

The primary motivation of this study was to improve on the status quo of 'static' maps by developing a 'dynamic' map that captures the spatial and temporal dynamics of HSAs at regional scales.

ERS data have been used previously to map and monitor changes in surface hydrological conditions over time (e.g. Kasischke *et al.* 2003). In this study, we extended the use of ERS data to calculate the probability of HSA occurrence for a 10-year period. A map of the probability of HSA occurrence for the entire drainage basin is presented in figure 7. This map showed that the majority of the drainage basin had a relatively small probability of HSA occurrence, with areas of medium to high probabilities in good agreement with previously mapped wetlands and riparian areas. The topographic effects associated with steep local slopes are evident along some of the southern river channels where enhanced backscattering occurred. The generally small probability of HSA occurrence is perhaps not surprising given that the watershed lies in a semiarid climatic zone. Moreover, the climatic trends of the past 30 years (figure 6) revealed that the past two decades were much drier than the 1970s. The probability map developed in this study captures a generally dry period. A broader temporal window of SAR data is therefore needed to capture longer-term climatic trends.

A closer inspection of the HSA probability map revealed substantial heterogeneity in the probability of formation of HSAs. Some areas remained consistently

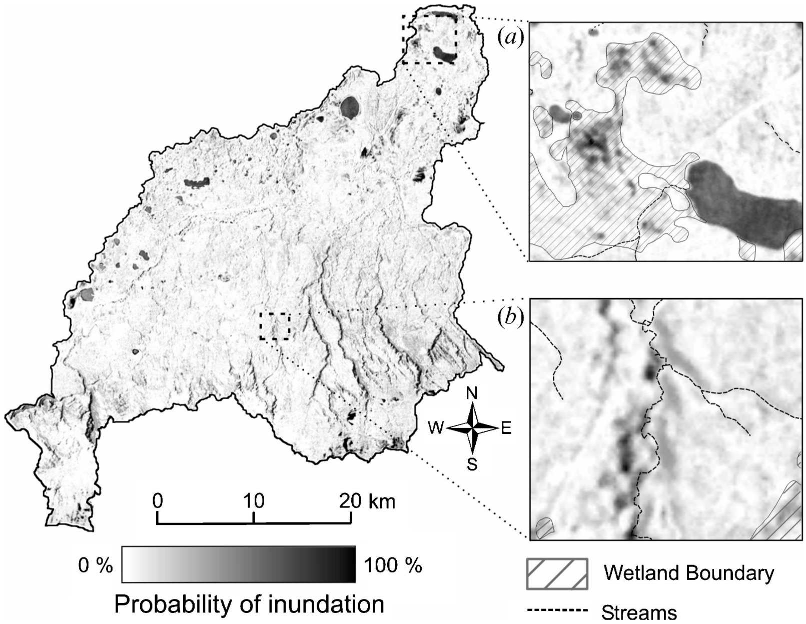

Figure 7. HSA probability map for the Willow River watershed illustrating the spatial and temporal dynamics encountered over a 10-year period. The topographic effects associated with steep local slopes are evident along some of the southern river channels where enhanced backscattering occurred. The two enlarged areas illustrate the dynamics associated with (*a*) a low-lying landscape and (*b*) a headwater stream. Wetland boundaries shown only on enlargements were mapped from the National Topographic Systems wetland layer.

dry, others consistently wet, while some areas were dynamic, transitioning from wet to dry and *vice versa*. For example, the enlargements in figure 7 show the HSA patterns associated with a large wetland area and a riverine setting, respectively.

The probability map offers the advantage of providing predictive information as well as representing the spatial and temporal dynamics of HSAs. To demonstrate the advantage we compared our 'dynamic' map with a currently available 'static' map by overlaying Canada's NTS (1 : 50 000) wetland layer onto our HSA probability map (figure 7, enlargements only). Referring to figure 7(*a*), we see a large wetland area represented by both the NTS wetland map and the HSA probability map. However, the probability map offers insight into both the temporal and spatial dynamics within the wetland, highlighting regions that were permanently wet (i.e. high probability) as well as regions that were dynamic (i.e. medium probability). Referring to figure 7(*b*), the probability map highlights the dynamic nature of HSAs in a riverine riparian zone, an important HSA that is not captured by the NTS wetland layer. The NTS wetland layer was derived through photointerpretation of aerial photographs based on plant indicators and soil characteristics, and does not necessarily capture the aerial extent of saturation or inundation, nor does it elucidate the temporal variation in the hydrological conditions experienced within the wetland. Clearly, the ERS-based mapping of HSAs offers valuable spatial and temporal hydrological information that is not currently available.

The technique showcased in this study offers potential for improved best land management practices. Incorporating probability of HSA occurrence into management decisions allows resource managers the opportunity to develop plans based on a defined level of risk of HSA occurrence. This includes the design and analysis of land management alternatives for minimizing nutrient loading to lakes and streams (Walter *et al.* 2000, Agnew *et al.* 2006), road placement (Wemple *et al.* 1996, Pulkki 2003) and overall forest operations planning (Andison 2003, Higman *et al.* 2005).

4.3 *Limitations of HSA detection*

We used ERS to detect dry *versus* wet (saturated or inundated) soils over a regional drainage basin. While our results clearly showed that the ERS images were sensitive to changes in wetness, we acknowledge, as previous studies have shown (e.g. Ulaby *et al.* 1996), that the microwave signal is also influenced by landscape properties, including topography and canopy. Currently, we lack the spatially distributed datasets (high-resolution digital elevation model (DEM) and vegetation structure data) to appropriately deal with the contributions of topography and vegetation to the observed microwave signal. We present a discussion of the hypothesized importance of these components in mapping HSAs in the Willow River watershed.

Local topographic effects on the backscatter response lead to errors in the radiometric calibration of SAR data (Van Zyl *et al.* 1993) and can mask the backscatter variation due to soil moisture by increasing dB values for slopes facing towards the satellite and lowering dB values for slopes facing away from the satellite (Hinse *et al.* 1988, Goyal *et al.* 1999). Inspection of the available coarse-resolution ($\approx$100 m) DEM (figure 8) indicated that slopes facing the satellite did enhance the backscatter but mostly in the southern headwater portion of the watershed

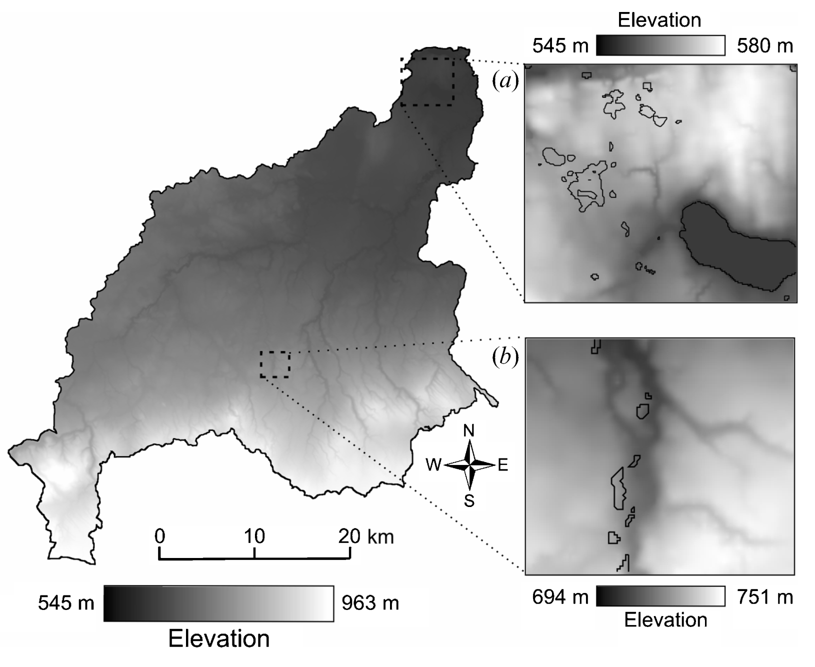

Figure 8. Digital elevation model for Willow River watershed. Enlargements show (*a*) a low-lying landscape and (*b*) a headwater stream (as in figure 7). Polygons superimposed on enlarged maps show areas with a high probability (>20%) of inundation (mapped from HSA map in figure 7).

(figure 8(*b*)). It was in this hillier region of the watershed where local slopes greater than 5° were located. Overall, slopes greater than 5° accounted for less than 10% of the total watershed area. However, even in these headwater valleys, the HSA probability map showed 'wetness' on slopes facing away from the satellite (figure 7(*b*)), which would be unexpected if terrain only influenced the backscatter signal. There were no notable topographic enhancements of the backscatter signal in the flatter northern portion of the drainage basin (figure 8(*a*)).

Vegetation effects on the backscatter response from canopy scattering and attenuation of the signal through the canopy (Dobson and Ulaby 1998) can mask the soil moisture signal. We assumed that the canopy allowed sufficient penetration of the microwave signal and did not preclude the detection of HSAs. We felt justified in making this assumption for the following reasons. First, the mixed wood boreal forest has relatively simple and open canopy structures. For example, only 5% of the forest has a canopy closure of 71–100%. Of the remaining forest, 10% has a canopy closure of 6–30%, 25% has a canopy closure of 31–50%, leaving 50% with a canopy closure of 51–71% (Alberta Vegetation Inventory 2003). Comparing the average probability of HSA occurrence in each canopy closure class showed no significant differences between classes. We also compared the spatial distribution of vegetation classes with the HSA probability map. In the low-lying area (figure 9(*a*)), areas with a high probability of inundation all fell within the black spruce vegetation class, which is associated with wet areas in this region. In the hillier headwater region (figure 9(*b*)), areas with a high probability of inundation were coincident with

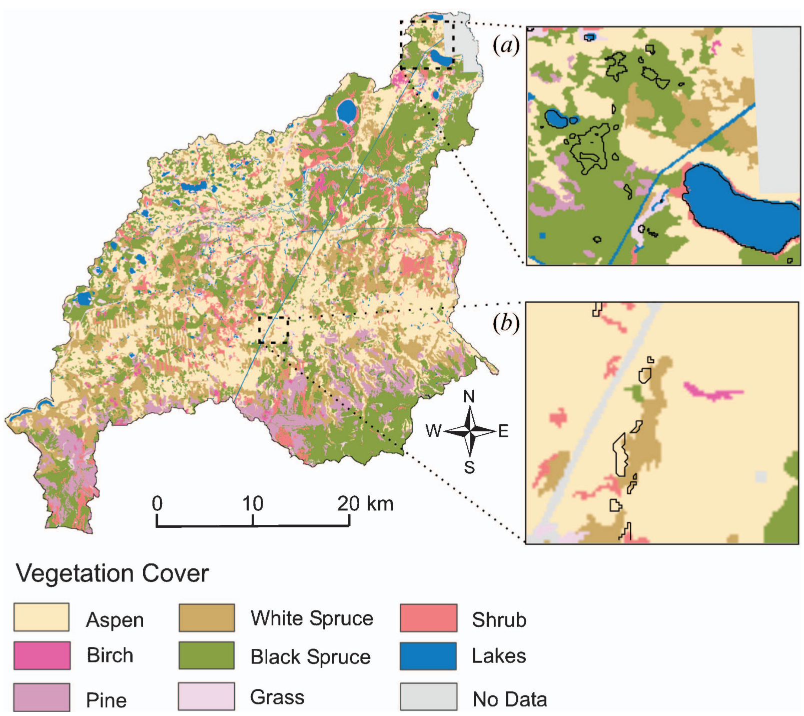

Figure 9. Vegetation cover map for Willow River watershed. Enlargements show (*a*) a low-lying landscape and (*b*) a headwater stream (as in figure 7). Polygons superimposed on enlarged maps show areas with a high probability (>20%) of inundation (mapped from HSA map in figure 7).

a mixture of white spruce and aspen vegetation classes. It is possible that the signal here is responding to vegetation scattering (in addition to topographic effects). However, it is also true that aspen and white spruce vegetation classes do not show a uniform HSA signal, which would be expected if the signal was dominated only by vegetation scattering.

A related study on the western Boreal Plain also provides empirical support for our assumptions. Sass and Creed (2008) conducted ground-based measurements of volumetric soil moisture content coincident with ERS image acquisition for a range of hydrological conditions under a similar canopy cover. They developed a relationship between the ERS backscatter coefficient and three hydrological classes (unsaturated, saturated and inundated) defined by volumetric soil moisture. When they tested this relationship on an independent data set they found that they were able to achieve an 88% success rate in using ERS images to classify dry *versus* wet conditions on the ground over a season.

Clearly, topography, vegetation and soil moisture all influence the backscatter signal. However, in this landscape we feel justified in not explicitly correcting for vegetation and topography because most of the hydrological action takes place in wetlands where canopies are sparse or absent and where the topography is flat. Future work will focus on incorporating vegetation and topography into HSA mapping at regional scales. The major impediment at this point is the availability of spatially distributed, fine-resolution data sets on topography and vegetation structure.

5. Conclusions

Maps of HSAs at regional scales are important for achieving best land management practices. A challenge for researchers is to develop tools that capture the spatial and temporal dynamics of HSAs at scales relevant to resource managers. We presented a remote sensing technique that used archived ERS-1 and ERS-2 images that were representative of the hydrological variability over a 10-year period to map HSAs for a remote watershed in the western boreal forest of Alberta, Canada. A map of the probability of HSA occurrence provides a simple yet powerful tool that may expand our understanding of the hydrological behaviour of drainage basins and serve as a planning tool for land management decisions.

Acknowledgements

Funding for this study was provided by a NSERC-CRD grant to S. Bayley, I. Creed, K. Devito and L. Foote for the Hydrology, Ecology, and Disturbance (HEAD) research project in collaboration with Ducks Unlimited Canada, Alberta-Pacific Forest Industries Inc, Weyerhaeuser Canada, Syncrude Canada Ltd, and Suncor Energy Inc. Funding was also provided by a Network of Centres of Excellence on Sustainable Forest Management (NCE-SFM) grant to I. Creed. We gratefully acknowledge NASA and the Alaska Satellite Facility for providing the ERS images.

References

ADAM, J.W., COLLINS, M. and PIETRONIRO, A., 1998, Radarsat flood mapping in the Peace-Athabasca Delta, Canada. *Canadian Journal of Remote Sensing*, **24**, pp. 69–79.

AGNEW, L.J., LYON, S., GÉRARD-MARCHANT, P., COLLINS, V.B., LEMBO, A.J., STEENHUIS, T.S. and WALTER, M.T., 2006, Identifying hydrologically sensitive areas:

bridging the gap between science and application. *Journal of Environmental Management*, **78**, pp. 63–76.

ANDISON, D.W., 2003, Tactical forest planning and landscape design. In *Towards Sustainable Management of the Boreal Forest*, W.L. Adamowicz (Ed.), pp. 433–480 (Ottawa: NRC Research Press).

ASF, 2004, *Alaska Satellite Facility Software Tools: The Use of the ASF Convert Tool* (Fairbanks, Alaska: Geophysical Institute, University of Alaska Fairbanks) Available online at: www.asf.alaska.edu.

BINDLISH, R. and BARROS, A.P., 2000, Multifrequency soil moisture inversion from SAR measurements with the use of IEM. *Remote Sensing of Environment*, **71**, pp. 67–88.

BOURGEAU-CHAVEZ, L.L., SMITH, K.B., BRUNZELL, S.M., KASISCHKE, E.S., ROMANOWICZ, E.A. and RICHARDSON, C.J., 2005, Remote monitoring of regional inundation patterns and hydroperiod in the greater everglades using synthetic aperture radar. *Wetlands*, **25**, pp. 176–191.

BRIVIO, P.A., COLOMBO, R., MAGGI, M. and TOMASONI, R., 2002, Integration of remote sensing data and GIS for accurate mapping of flooded areas. *International Journal of Remote Sensing*, **23**, pp. 429–441.

BRUN, C., BERNARD, R., VIDAL-MADJAR, D., GASCUEL-ODOUX, C., MEROT, P., DUCHESNE, J. and NICOLAS, H., 1990, Mapping saturated areas with a helicopter-borne C band scatterometer. *Water Resources Research*, **26**, pp. 945–955.

BURROUGH, P.A., and MCDONNELL, R.A. (Eds), 1998, *Principals of Geographical Information Systems: Spatial Information Systems and Geostatistics*, pp. 265–291 (New York: Oxford University Press).

BUTTLE, J.M., CREED, I.F. and MOORE, R.D., 2005, Progress in Canadian forest hydrology: 1999–2003. *Hydrological Processes*, **19**, pp. 169–200.

CHAMPION, I. and FAIVRE, R., 1997, Sensitivity of the radar signal to soil moisture: variation with incidence angle, frequency, and polarization. *IEEE Transactions on Geoscience and Remote Sensing*, **35**, pp. 781–783.

CLARK, R.C., 2004, Mapping inundation on a forested landscape in the boreal forest – a multi-temporal analysis of ERS synthetic aperture radar data. MSc thesis, University of Western Ontario.

CREED, I.F. and BAND, L.E., 1998, Export of nitrogen from catchments within a temperate forest: evidence for a unifying mechanism regulated by variable source area dynamics. *Water Resources Research*, **34**, pp. 3105–3120.

CREED, I.F., BAND, L.E., FOSTER, N.W., MORRISON, I.K., NICOLAS, J.A., SEMKIN, R.S. and JEFFRIES, D.S., 1996, Regulation of nitrate-N release from temperate forests: a test of the N flushing hypothesis. *Water Resources Research*, **32**, pp. 3337–3354.

CREED, I.F., SANFORD, S.E., BEALL, F.D., MOLOT, L.A. and DILLON, P.J., 2003, Cryptic wetlands: integrating hidden wetlands in regression models of the export of dissolved organic carbon from forested landscapes. *Hydrologic Processes*, **17**, pp. 3629–3648.

DEVITO, K.J., CREED, I.F., ROTHWELL, R.L. and PREPAS, E.E., 2000, Landscape controls on phosphorus loading to boreal lakes: implications for the potential impacts of forest harvesting. *Canadian Journal of Fisheries and Aquatic Sciences*, **57**, pp. 1977–1984.

DOBSON, M.C. and ULABY, F.T., 1986, Active microwave soil moisture research. *IEEE Transactions on Geoscience and Remote Sensing*, **24**, pp. 23–36.

DOBSON, M.C. and ULABY, F.T., 1998, Mapping soil moisture distribution with imaging radar. In *Principals and Applications of Imaging Radar: Manual of Remote Sensing*, 3rd edn, vol. 2, F.M. Henderson, and A.J. Lewis (Eds), pp. 407–433 (New York: John Wiley and Sons Inc).

ECOLOGICAL STRATIFICATION WORKING GROUP, 1996, *A National Ecological Framework for Canada* (Ottawa/Hull: Agriculture and Agri-Food Canada, Research Branch, Centre for Land and Biological Resources Research and Environment Canada, State of Environment Directorate).

GINESTE, P., PUECH, C. and MÉROT, P., 1998, Radar remote sensing of source areas from the Coët-Dan catchment. *Hydrological Processes*, **12**, pp. 267–284.

GOYAL, S.K., SEYFRIED, M.S. and O'NEILL, P.E., 1999, Correction of surface roughness and topographic effects on airborne SAR in mountainous rangeland areas. *Remote Sensing of Environment*, **67**, pp. 124–136.

HAMON, R.W., 1964, Computation of direct runoff amounts from storm rainfall. In *Symposium on Surface Waters*, pp. 52–62. IAHS Publication no. 63 (Wallingford: IAHS Press).

HESS, L.L., MELACK, J.M., FILOSO, S. and WANG, Y., 1995, Delineation of inundated area and vegetation along the Amazon floodplain with the SID-C synthetic aperture radar. *IEEE Transactions on Geoscience and Remote Sensing*, **33**, pp. 896–904.

HESS, L.L., MELACK, J.M., NOVO, E.M.L.M., BARBOSA, C.C.F. and GASTIL, M., 2003, Dual-season mapping of wetland inundation and vegetation for the central Amazon basin. *Remote Sensing of Environment*, **87**, pp. 404–428.

HESS, L.L., MELACK, J.M. and SIMONETT, D.S., 1990, Radar detection of flooding beneath the forest canopy: a review. *International Journal of Remote Sensing*, **11**, pp. 1313–1325.

HIGMAN, S., MAYERS, J., BASS, S., JUDD, N., and NUSSBAUM, R. (Eds), 2005, *The Sustainable Forestry Handbook*, pp. 160–180 (London: Earthscan).

HINSE, M., GWYN, Q.H.J. and BONN, F., 1988, Radiometric correction of C-band imagery for topographic effects in regions of moderate relief. *IEEE Transactions on Geoscience and Remote Sensing*, **26**, pp. 122–132.

HOBSON, K.A., BAYNE, E.M. and VAN WILGENBURG, S.L., 2002, Large-scale conversion of forest to agriculture in the boreal plains of Saskatchewan. *Conservation Biology*, **16**, pp. 1530–1541.

HORRITT, M.S., MASON, D.C., COBBY, D.M., DAVENPORT, I.J. and BATES, P.D., 2003, Waterline mapping in flooded vegetation from airborne SAR imagery. *Remote Sensing of Environment*, **85**, pp. 271–281.

HORRITT, M.S., MASON, D.C. and LUCKMAN, A.J., 2001, Flood boundary delineation from synthetic aperture radar imagery using a statistical active contour model. *International Journal of Remote Sensing*, **22**, pp. 2489–2507.

KASISCHKE, E.S., SMITH, K.B., BOURGEAU-CHAVEZ, L.L., ROMANOWICZ, E.A., BRUNZELL, S. and RICHARDSON, C.J., 2003, Effects of seasonal hydrologic patterns in south Florida wetlands on radar backscatter measured from ERS-2 SAR imagery. *Remote Sensing of Environment*, **88**, pp. 423–441.

LEIBOWITZ, S.G. and VINING, K.C., 2003, Temporal connectivity in a prairie pothole complex. *Wetlands*, **23**, pp. 13–25.

LINDSAY, J.B., 2005, The terrain analysis system: a tool for hydro-geomorphic applications. *Hydrological Processes*, **19**, pp. 1123–1130.

LOPES, A., NEZRY, E., TOUZI, R. and LAUR, H., 1993, Structure detection and statistical adaptive speckle filtering in SAR images. *International Journal of Remote Sensing*, **14**, pp. 1735–1758.

MEADOWS, P.J., ROSICH, B. and SANTELLA, C., 2004, The ERS-2 SAR performance: the first 9 years. In *Proceedings of the ENVISAT and ERS Symposium*, 6–10 September 2004, Salzburg, Austria, H. Lacoste and L. Ouwehand (Eds.), ESA SP-572.

MÉROT, P., CRAVE, A. and GASCUEL-ODOUX, C., 1994, Effects of saturated areas on backscattering coefficient of the ERS 1 synthetic aperture radar: first results. *Water Resources Research*, **30**, pp. 175–179.

MORRISSEY, L.A., DURDEN, S.L., LIVINGSTON, G.P., STEARN, J.A. and GUILD, L.S., 1996, Differentiating methane source areas in arctic environments with multitemporal ERS-1 SAR data. *IEEE Transactions on Geoscience and Remote Sensing*, **34**, pp. 667–673.

OLDAK, A., JACKSON, T.J., STARKS, P. and ELLIOTT, R., 2003, Mapping near-surface soil moisture on regional scale using ERS-2 SAR data. *International Journal of Remote Sensing*, **24**, pp. 4579–4598.

PAULEN, R.C., FENTON, M.M. and PAWLOWICZ, J.G., 2004a, *Surficial Geology of the Utikuma Area (NTS 83O/NW), Scale 1 : 100,000.* Alberta Energy and Utilities Board, EUB/AGS Map 312 (Edmonton, Alberta, Canada: Alberta Geological Survey, Alberta Energy and Utilities Board).

PAULEN, R.C., FENTON, M.M. and PAWLOWICZ, J.G., 2004b, *Surficial Geology of the Willow River Area (NTS 83O/NE). Scale 1 : 100,000.* Alberta Energy and Utilities Board, EUB/AGS Map 313 (Edmonton, Alberta, Canada: Alberta Geological Survey, Alberta Energy and Utilities Board).

PIETRONIRO, A. and LECONTE, R., 2003, Applications of remote sensing in hydrology. *Hydrological Processes*, **16**, pp. 1537–1541.

PIETRONIRO, A. and LECONTE, R., 2005, A review of Canadian remote sensing and hydrology, 1999–2003. *Hydrological Processes*, **19**, pp. 285–301.

POPE, K.O., REJMANKOVA, E., PARIS, J.F. and WOODRUFF, R., 1997, Detecting seasonal flooding cycles in marshes of the Yucatan Peninsula with SIR-C polarimetric radar imagery. *Remote Sensing of Environment*, **59**, pp. 157–166.

PULKKI, R., 2003, Minimizing negative environmental impacts of forest harvesting operations. In *Towards Sustainable Management of the Boreal Forest*, P.J. Burton, C. Messier, D.W. Smith and L.A. Wiktor (Eds), pp. 581–628 (Ottawa: NRC Research Press).

PULLIAINEN, J.T., MIKKELÄ, P.J., HALLIKAINEN, M.T. and IKONEN, J.P., 1996, Seasonal dynamics of C-band backscatter of boreal forests with applications to biomass and soil moisture estimation. *IEEE Transactions on Geoscience and Remote Sensing*, **34**, pp. 758–770.

RICHARDS, J.A., WOODGATE, P.W. and SKIDMORE, A.K., 1987, An explanation of enhanced radar backscattering from flooded forests. *International Journal of Remote Sensing*, **8**, pp. 1093–1100.

RIGNOT, E.J. and VAN ZYL, J.J., 1993, Change detection techniques for ERS-1 SAR data. *IEEE Transactions on Geoscience and Remote Sensing*, **31**, pp. 896–906.

ROSENQVIST, A., FORSBERG, B.R., PIMENTEL, T., RAUSTE, Y.A. and RICHEY, J.E., 2002, The use of spaceborne radar data to model inundation patterns and trace gas emissions in the central Amazon floodplain. *International Journal of Remote Sensing*, **23**, pp. 1303–1328.

RUSTOMJI, P. and PROSSER, I., 2001, Spatial patterns of sediment delivery to valley floors: sensitivity to sediment transport capacity and hillslope hydrology relations. *Hydrological Processes*, **15**, pp. 1003–1018.

SASS, G.Z. and CREED, I.F., 2008, Characterizing hydrodynamics on boreal landscapes using archived synthetic aperture radar imagery. *Hydrological Processes*, **22**, pp. 1687–1699.

SCHINDLER, D.W., 1998, A dim future for boreal water and landscapes. *BioScience*, **48**, pp. 157–164.

SCHINDLER, D.W., 2001, The cumulative effects of climate warming and other human stresses on Canadian freshwaters in the new millennium. *Canadian Journal of Fisheries and Aquatic Sciences*, **58**, pp. 18–29.

SCHMUGGE, T.J., 1980, Effect of texture on microwave emission from soils. *IEEE Transactions on Geoscience and Remote Sensing*, **18**, pp. 353–361.

TOWNSEND, P.A., 2001, Mapping seasonal flooding in forested wetlands using multi-temporal Radarsat SAR. *Photogrammetric Engineering and Remote Sensing*, **67**, pp. 857–864.

TROCH, P., VERHOEST, N., GINESTE, P., PANICONI, C. and MÉROT, P., 2000, Variable source areas, soil moisture and active microwave observations at Zwalmbeek and Coët-Dan. In *Spatial Patterns in Catchment Hydrology: Observations and Modeling*, R.B. Grayson and G. Blöschl (Eds), pp. 187–208 (Cambridge: Cambridge University Press).

ULABY, F.T., DUBOIS, P.C. and VAN ZYL, J., 1996, Radar mapping of surface soil moisture. *Journal of Hydrology*, **184**, pp. 57–84.

VAN ZYL, J.J., CHAPMAN, B.D., DUBOIS, P. and SHI, J., 1993, The effect of topography on SAR calibration. *IEEE Transactions on Geoscience and Remote Sensing*, **31**, pp. 1036–1043.

VERHOEST, N.E., TROCH, P.A., PANICONI, C. and DE TROCH, F.P., 1998, Mapping basin scale variable source areas from multitemporal remotely sensed observations of soil moisture behavior. *Water Resources Research*, **34**, pp. 3235–3244.

WALTER, M.T., WALTER, M.F., BROOKS, E.S., STEENHUIS, T.S., BOLL, J. and WEILER, K., 2000, Hydrologically sensitive areas: variable source area hydrology implications for water quality risk assessment. *Journal of Soil and Water Conservation*, **55**, pp. 277–286.

WANG, Y., HESS, L.L., FILOSO, S. and MELACK, J.M., 1995, Understanding the radar backscattering from flooded and nonflooded Amazonian forests: results from canopy backscatter modeling. *Remote Sensing of Environment*, **54**, pp. 324–332.

WEMPLE, B.C., JONES, J. and GRANT, G.E., 1996, Channel network extension by logging roads in two basins, western cascades, Oregon. *Water Resources Bulletin*, **32**, pp. 1195–1207.

WICKEL, A.J., JACKSON, T.J. and WOOD, E.F., 2001, Multitemporal monitoring of soil moisture with Radarsat SAR during the 1997 Southern Great Plains hydrology experiment. *International Journal of Remote Sensing*, **22**, pp. 1571–1583.

ZADEH, L.A., 1965, Fuzzy sets. *Information and Controls*, **8**, pp. 338–353.